

Dalton Transactions

Accepted Manuscript



This is an *Accepted Manuscript*, which has been through the Royal Society of Chemistry peer review process and has been accepted for publication.

Accepted Manuscripts are published online shortly after acceptance, before technical editing, formatting and proof reading. Using this free service, authors can make their results available to the community, in citable form, before we publish the edited article. We will replace this *Accepted Manuscript* with the edited and formatted *Advance Article* as soon as it is available.

You can find more information about *Accepted Manuscripts* in the [Information for Authors](#).

Please note that technical editing may introduce minor changes to the text and/or graphics, which may alter content. The journal's standard [Terms & Conditions](#) and the [Ethical guidelines](#) still apply. In no event shall the Royal Society of Chemistry be held responsible for any errors or omissions in this *Accepted Manuscript* or any consequences arising from the use of any information it contains.

Phase evolution and microwave dielectric properties of $x\text{Bi}_{2/3}\text{MoO}_4-(1-x)\text{BiVO}_4$ ($0.0 \leq x \leq 1.0$) low temperature firing ceramics

Di Zhou,^{*a} Wen-Bo Li,^a Li-Xia Pang,^b Jing Guo,^a Ze-Ming Qi,^c Tao Shao,^c Xi Yao^a
and Clive A. Randall^d

^aElectronic Materials Research Laboratory, Key Laboratory of the Ministry of Education & International Center for Dielectric Research, Xi'an Jiaotong University, Xi'an 710049, Shaanxi, China

^bMicro-optoelectronic Systems Laboratories, Xi'an Technological University, Xi'an 710032, Shaanxi, China

^cNational Synchrotron Radiation Laboratory, University of Science and Technology of China, Hefei, Anhui, 230029, China

^dThe Pennsylvania State University, Center for Dielectric Studies, Materials Research Institute, University Park, PA 16802, USA

Abstract

In the present work, a full composition of $x\text{Bi}_{2/3}\text{MoO}_4-(1-x)\text{BiVO}_4$ ($0.0 \leq x \leq 1.0$) was prepared by the solid state reaction method. All the ceramic compositions could be readily densified to below 850 °C. As the x value increased, the monoclinic scheelite structure continuously changed to a tetragonal structure at $x=0.10$, which means the ferroelastic phase transition temperature was lowered to near room temperature. In the

*Corresponding author. Tel. (Fax.): +86-29-82668679; E-mail address: zhoudi1220@gmail.com (Di Zhou)

compositional range $0.50 \leq x < 0.70$, a novel ordered scheelite phase was formed, most likely through A-site vacancy ordering. For compositions $x \geq 0.70$, a composite two-phase region consisting of the ordered scheelite and $\text{Bi}_{2/3}\text{MoO}_4$ phases was formed. High microwave permittivity around 75 and Qf values around 8,000 GHz could be obtained in the compositions near the phase boundaries between monoclinic and tetragonal scheelite phases. The intrinsic microwave dielectric properties were extrapolated from the far infrared reflectivity spectra, and it was found that the polarization was dominated by the Bi-O stretches when $x \leq 0.10$.

I. Introduction

With the rapid development of mobile communication, satellite communication, Global Position System (GPS), and Wireless Local Area Network (WLAN) technology, the low temperature co-fired ceramic (LTCC) technology has played an important role in the fabrication of microwave devices to meet the requirements of miniaturization and integration, due to its advantage in designing every layer separately and co-firing the dielectric and electrode layers together.¹⁻³

Usually, most traditional microwave dielectrics with high performance have high sintering temperature and cannot be employed in LTCC technology. Over a couple of decades, there was a large amount of work carried out to lower the sintering temperature of high temperature sintered microwave dielectric ceramics. Besides the addition of sintering aids and the usage of ultra-fine initial powders, a novel, fruitful approach is to search for new compounds with intrinsic low sintering temperatures.⁴⁻⁶

Bismuth-based microwave dielectric ceramics have attracted much attention due to their low intrinsic sintering temperature and large permittivity (polarizability of Bi^{3+} is 6.12 \AA^3).^{7,8} The two classic bismuth-based microwave dielectric ceramics with

pyrochlore-related structures are $(\text{Bi}_{1.5}\text{Zn}_{0.5})(\text{Zn}_{0.5}\text{Nb}_{1.5})\text{O}_7$ (α -BZN) and $\text{Bi}_2(\text{Zn}_{2/3}\text{Nb}_{4/3})\text{O}_7$ (β -BZN),^{9,10} which can be densified ~ 960 °C with high permittivity 160 and 80, respectively. However, these pyrochlores have a relatively low quality factor ($Q_f = 300$ GHz and 4,000 GHz, respectively), limiting their application in microwave devices. Besides, the high sintering temperature (above 960 °C) also caused the volatilization of bismuth in ceramics. The traditional BiVO_4 material is used as an important kind of yellow dye in place of former lead chromium yellow with heavy metals contents which is harmful to human being body.¹¹ Recently, the BiVO_4 with distorted monoclinic scheelite structure has also attracted attention due to its high performance microwave properties (permittivity ~ 68 , Q_f around 8,000 GHz) and low intrinsic sintering temperature below 900 °C, which made the volatilization problem under control.⁷ The BiVO_4 material was reported to undergo a reversible second order ferroelastic phase transition (monoclinic scheelite \leftrightarrow tetragonal scheelite), which can be induced by high temperature about 255 °C or high pressure about 16 k bar.^{12,13} It was found that this phase transition can also be achieved by introducing larger ions than V^{5+} at B-site, and the phase transition temperature can be lowered to near room temperature, as shown in our recent research.^{6,14,15} Furthermore, excellent microwave dielectric properties can be reached in the compositions near the phase boundary, such as $[(\text{Li}_{0.5}\text{Bi}_{0.5})_{0.098}\text{Bi}_{0.902}][\text{Mo}_{0.098}\text{V}_{0.902}]\text{O}_4$ ceramic sintered at 650 °C with a permittivity ~ 81 , a $Q_f \sim 8,000$ GHz, and $0.1\text{Bi}(\text{Fe}_{1/3}\text{Mo}_{2/3})\text{O}_4$ - 0.9BiVO_4 sintered at 820 °C with a permittivity ~ 74.8 and a $Q_f \sim 11,600$ GHz.^{6,16}

The general formula for scheelite (CaWO_4) oxides is ABO_4 , in which the A cation is octahedrally coordinated to oxygen, while the B cation is tetrahedrally coordinated, and crystal structure details can be found in literatures.^{14,17} It was reported that large

concentrations of metal vacancies point defect could be introduced to A-site when donor doped, D, with a trivalent cation, for example, and so the general chemical formula for scheelite becomes $(A^{+2}_{1-3x/2}D^{+3}_x)BO_4$. For the special case of $x = 2/3$, we have a maximum of $1/3$ vacancies on the A-site, assuming full ionic compensation with the donor and the metal vacancies, $[D^\bullet]=2[Vm'']$. Such examples are $La_{2/3}MoO_4$ that is disordered vacancy distribution when quenched from high temperatures, and ordered cation vacancies on naturally cooling sample. In this case, the MoO_4 tetrahedra were more distorted than that in the ideal tetragonal scheelite structure.¹⁷⁻¹⁹ Similarly, in the case of pure $Bi_{2/3}MoO_4$, the A-site vacancies take on an ordered arrangement, and it was indexed in a scheelite related monoclinic structure with space group $P2_1/c$.^{20,21} In our previous work, the $Bi_{2/3}MoO_4$ ($Bi_2Mo_3O_{12}$) ceramic was found to possess a microwave dielectric permittivity ~ 19 , a Qf value $\sim 21,800$ GHz and a ultra-low sintering temperature around 620 °C. Hence, in the present work, a full composition study of $xBi_{2/3}MoO_4-(1-x)BiVO_4$ ($0.0 \leq x \leq 1.0$), was carried out, considering the phase transition, microwave dielectric properties, and their relationship with the crystal structure.

II. Experimental Methods

Proportionate amounts of reagent-grade starting materials of Bi_2O_3 ($> 99\%$, Shu-Du Powders Co. Ltd., Chengdu, China), V_2O_5 ($> 99\%$, Sinopharm Chemical Reagent Co., Ltd, Shanghai, China), and MoO_3 ($> 99\%$, Fuchen Chemical Reagents, Tianjin, China) were measured according to the stoichiometric formulation $xBi_{2/3}MoO_4-(1-x)BiVO_4$ ($0.0 \leq x \leq 1.0$) (abbreviated here as BVMx). Powders were mixed and milled for 4 h using a planetary mill (Nanjing Machine Factory, Nanjing, China) by setting the running speed at 150 rpm with the zirconia balls (2 mm in diameter) as milling media.

The powder mixture was then dried and calcined at 600~700 °C for 4hrs. The calcined powders were ball milled for 5hrs with a running speed at 200 rpm to obtain fine powders. Then the powders were pressed into cylinders (10 mm in diameter and 4 ~ 5 mm in height) in a steel die with 5wt. % PVA binder addition under a uniaxial pressure of 200 MPa. Samples were sintered in the temperature range from 620 °C to 830 °C for 2hrs. Room temperature XRD was performed using a XRD with CuK α radiation (Rigaku D/MAX-2400 X-ray diffractometry, Tokyo, Japan). Prior to examination, sintered pellets were crushed in a mortar and pestle to powder. Diffraction pattern was obtained between 5-65 ° (2 θ) at a step size of 0.02 °. The specimens for transmission electron microscope were prepared from the sintered pellets and examined using a JEOL 2100 TEM microscope operated at 200 kV. To examine the grain morphology, as-fired and fractured surfaces were examined by scanning electron microscopy (SEM) (JSM-6460, JEOL, Tokyo, Japan). The Raman spectra at room temperature were obtained on polished pellets with a Raman spectrometer (inVia, Renishaw, England), excited by an Ar⁺ laser (514.5 nm). The high temperature Raman spectra were measured using another Raman spectrometer (LabRAM HR800, HORIBA Jobin Yvon, France). The room temperature infrared reflectivity spectra were measured using a Bruker IFS 66v FTIR spectrometer on Infrared beamline station (U4) at National Synchrotron Radiation Lab. (NSRL), China. Dielectric properties at microwave frequency were measured with the TE₀₁₈ dielectric resonator method with a network analyzer (HP 8720 Network Analyzer, Hewlett-Packard) and a temperature chamber (Delta 9023, Delta Design, Poway, CA).

III Results and Discussions

The X-ray diffraction patterns for xBi_{2/3}MoO₄-(1-x)BiVO₄ (0.0 ≤ x ≤ 1.0) ceramics

sintered at different temperatures, the cell parameters as a function of x value, and the schematic structure of BiVO_4 and $\text{Bi}_{2/3}\text{MoO}_4$ with only half the unit cell shown in ab -plane are presented in Fig. 1. As to be expected, based on our previous investigations on $(\text{A}_{0.5x}\text{Bi}_{1-0.5x})(\text{Mo}_x\text{V}_{1-x})\text{O}_4$ ($\text{A} = \text{Li}, \text{Na}$ and K) and $x\text{Bi}(\text{Fe}_{1/3}\text{Mo}_{2/3})\text{O}_4-(1-x)\text{BiVO}_4$ systems,^{6,14,15} as x value increased from 0.02 to 0.10, small amounts of substitution with bigger ionic radius, such as Mo^{6+} and Fe^{3+} for V^{5+} , occur on the B-site of the ABO_4 composition. This results in the onset of a second order ferroelastic phase transition to tetragonal scheelite structure. Experimentally, the transition from monoclinic to tetragonal is noted by merging of X-ray powder diffraction peaks (1 0 1) and (0 1 1), (2 0 0) and (0 2 0), etc. As seen from Fig. 1 (a), this is common, irrespective of vacancies or cation substitution on the A site. This ferroelastic phase transition is believed to result from the increase of the atomic packing factor in monoclinic phase region for which the cell volume is dominated by the tetrahedron BO_4 network. As the x value increased to 0.50, a few super-lattice diffraction peaks could be observed beside the peaks of tetragonal scheelite (marked inside the box in Fig. 1 (b)). When the x value increased to 0.70, a trace of the main peaks of monoclinic $\text{Bi}_{2/3}\text{MoO}_4$ phase at 28.13° and 29.26° could be revealed, which indicates that the solid solubility of the single-phase tetragonal materials reached a maximum here. As x value further increased, the intensity of tetragonal scheelite peaks decreased, and pure monoclinic $\text{Bi}_{2/3}\text{MoO}_4$ phase was formed at $x=1.00$. It must be pointed out that the super-lattice peaks and phase composition in $x\text{Bi}_{2/3}\text{MoO}_4-(1-x)\text{BiVO}_4$ ($0.0 \leq x \leq 1.0$) ceramics were not influenced with annealing times, which indicates that the phase equilibrium can be easily reached here, and kinetics are relatively fast. The schematic diagram of the ideal scheelite structure, with vacancies less than $1/3$ on A-site and pure monoclinic $\text{Bi}_{2/3}\text{MoO}_4$ phase, are

shown in Fig. 1 (e). The phase transition from monoclinic to tetragonal scheelite structure can be attributed to the small amount substitution of Mo^{6+} for V^{5+} on the B-site with disordering arrangement. Meanwhile, the A site vacancy also arranges in a disordering manner. In the super-lattice region ($x \geq 0.50$), the vacancy and Bi^{3+} cations arrange in an ordered manner, and it can still be tolerated under the tetragonal scheelite structure. The solid solubility of the vacancy of Bi^{3+} on the A-site reaches a maximum about 23 mol. % in the tetragonal scheelite structure at $x=0.7$. With a further increase of x value, the tetragonal scheelite structure cannot hold any more vacancies, and a monoclinic $\text{Bi}_{2/3}\text{MoO}_4$ was formed to arrange the increasing Bi^{3+} vacancy. The maximum value of vacant A-site cations is $1/3$ in the scheelite-related defect structures, which can be represented as $(\text{A}^{+2}_{1-3x/2}\text{D}^{+3}_x)\text{BO}_4$, and the MoO_4 here are somewhat more distorted than that in the ideal tetragonal $\text{A}^{+2}\text{MoO}_4$ scheelites. Specially, the MoO_4 tetrahedra in $\text{Bi}_{2/3}\text{MoO}_4$ reaches a most distorted situation, as seen in Fig. 1 (e). A set of representative transmission electron diffraction patterns of selected area of BVM0.35 sample is shown in Fig 1 (f). All patterns were indexed according to a scheelite tetragonal unit cell with lattice parameters $a = b = 5.192 \text{ \AA}$ and $c = 11.701 \text{ \AA}$, which correspond well with the XRD results.

SEM micrographs of as-fired and fractured surfaces demonstrate the granular microstructure of the $x\text{Bi}_{2/3}\text{MoO}_4-(1-x)\text{BiVO}_4$ ceramics ($x = 0.06, 0.08, 0.10, 0.35, 0.65, \text{ and } 1.00$) sintered at different temperatures, as shown in Fig. 2. Dense and homogeneous microstructures with almost no pores could be revealed in all compositions. The densification temperature decreased almost linearly from $830 \text{ }^\circ\text{C}$ for BVM0.06 to about $620 \text{ }^\circ\text{C}$ for pure $\text{Bi}_{2/3}\text{MoO}_4$ ceramic. As seen from Fig. 2 (d), (e), and (f), the fractures changed gradually from a transgranular fracture to an intergranular one as x value increased from 0.35 to 1.00. This might be attributed to

the decreasing sintering temperature as x value increased, and the low relative density of pure $\text{Bi}_{2/3}\text{MoO}_4$ ceramic, in which the pores can more easily promote the intergranular fracture.

The room temperature Raman spectra of $x\text{Bi}_{2/3}\text{MoO}_4-(1-x)\text{BiVO}_4$ ($0.0 \leq x \leq 1.0$) ceramics are shown in Fig. 3 (a). Similar results to previous work are obtained here for pure BiVO_4 .^{14,15} The intense Raman band near 824.4 cm^{-1} is assigned to $\nu_s(\text{V}-\text{O})$, and with a weak shoulder at about 713.6 cm^{-1} is assigned to $\nu_{as}(\text{V}-\text{O})$. The symmetric A_g bending mode of vanadate anion $\delta_s(\text{VO}_4^{3-})$ and the anti-symmetric B_g bending mode of vanadate anion $\delta_{as}(\text{VO}_4^{3-})$ modes are near 366.8 and 325.3 cm^{-1} , respectively, and external modes (rotation/translation) occur near 211.9 cm^{-1} and 127.2 cm^{-1} , respectively. Since ferroelastic phase transition can be induced here, the characteristic merging of the $\delta_s(\text{VO}_4)$ (B_g) and $\delta_{as}(\text{VO}_4)$ (A_g) modes at around 366.8 and 325.3 cm^{-1} for pure BiVO_4 to one at 340.2 cm^{-1} for BVM0.10 could be observed, which is similar to the our previous results.⁶ The *in-situ* Raman spectra of BVM0.06 sample in the temperature range $25 \sim 200 \text{ }^\circ\text{C}$ are shown in Fig. 2(b). It is observed that as the temperature increased and the $\delta_s(\text{VO}_4)$ and $\delta_{as}(\text{VO}_4)$ modes moved closer to each other, they finally became a single peak at about $105 \text{ }^\circ\text{C}$. This result is consistent with the existence of the ferroelastic phase transition in $x\text{Bi}_{2/3}\text{MoO}_4-(1-x)\text{BiVO}_4$ system and its dependence on both composition and temperature. For the pure $\text{Bi}_{2/3}\text{MoO}_4$, the sharp bands at 926.6 , 900.6 , 858.3 , 840.4 , 815.8 , and 648.7 cm^{-1} are assigned to the Mo-O stretching modes, and the bands at 160.8 , 194.3 , and 366.8 cm^{-1} are assigned to the bending/wagging and external modes (and possible Bi-O stretches), which is similar to other reports in the literatures.²²⁻²⁴ In particular, the excellent work of Hardcastle and Wachs's²² considered detailed assignments of the Raman bands, and the relationship between Raman spectra, molybdenum coordinations, and Mo-O bond

lengths. As the Mo content increased with x value, the Mo-O stretching band at around 876.3 cm^{-1} became stronger and replaces the V-O stretching band at 820 cm^{-1} as the new strongest one at $x=0.65$. The Raman spectra are sensitive to the ordered structure, and a new band at around 604 cm^{-1} was observed for $x = 0.55, 0.65,$ and 0.70 samples. Based on the Bi^{3+} vacancy ordering from XRD analysis, the band at 604 cm^{-1} is understandable and may be assigned to Bi-O stretches and medium-range order. For BVM0.90 sample, it is seen that the spectra are mixtures of both BVM0.70 and BVM1.00, which further confirms the XRD results. The black spectra below that of BVM0.90 was obtained by subtracting pure spectra of $\text{Bi}_{2/3}\text{MoO}_4$, and it is similar to the spectra of $x = 0.55, 0.65$ and 0.70 sample.

Figure 4 shows the room temperature microwave dielectric properties of $x\text{Bi}_{2/3}\text{MoO}_4-(1-x)\text{BiVO}_4$ ($0.0 \leq x \leq 1.0$) ceramics as a function of x value (at $4.8 \sim 8.5$ GHz). The microwave permittivity first increased linearly from 69 to a maximum value ~ 75 as x value increased from 0.0 to 0.06, and then decreased down to 19.6 for end member $\text{Bi}_{2/3}\text{MoO}_4$. This agrees well with the rule that the maximum value of permittivity can be obtained in the compositions near the phase boundary of monoclinic and tetragonal phases due to the decrease of the cell volume.^{6,15} The Qf values kept stable about 8,000 GHz in the range $0.0 \leq x \leq 0.35$. Then it decreased to around 6,000 GHz for $x = 0.55, 0.65,$ and 0.70 , and this might be attributed to the ordered arrangement of Bi^{3+} vacancy. Finally, the Qf value increased sharply from 8,000 GHz for BVM0.90 to around 21,000 GHz for pure $\text{Bi}_{2/3}\text{MoO}_4$ ceramic.

The temperature dependence of microwave dielectric permittivity and Qf value of $x\text{Bi}_{2/3}\text{MoO}_4-(1-x)\text{BiVO}_4$ ($x = 0.06, x = 0.08, x = 0.10,$ and $x = 0.35$) ceramics are shown in Fig. 5. It can be seen that the expected maximum value of relative permittivity as a function of temperature could be observed in samples with $x = 0.06$,

$x = 0.08$, and $x = 0.10$, which means that the ferroelastic phase transition temperature in $x\text{Bi}_{2/3}\text{MoO}_4-(1-x)\text{BiVO}_4$ ceramics decreased from $113\text{ }^\circ\text{C}$ at $x = 0.06$ to $29\text{ }^\circ\text{C}$ at $x = 0.10$. When x value increased to 0.35 , there is no obvious peak observed; even the temperature is as low as $-250\text{ }^\circ\text{C}$ and the microwave dielectric permittivity almost decreased linearly with the temperature, which means that the monoclinic scheelite structure cannot be formed in this composition. This result is also similar to the situation in $x\text{Bi}(\text{Fe}_{1/3}\text{Mo}_{2/3})\text{O}_4-(1-x)\text{BiVO}_4$ system.⁶ It seems that the Q_f values decreased sharply with the temperature when $x \leq 0.10$ and the introduction of $\text{Bi}_{2/3}\text{MoO}_4$ improve the temperature stability of Q_f value.

Figure 6 presents the room temperature IR reflectivity spectra of $x\text{Bi}_{2/3}\text{MoO}_4-(1-x)\text{BiVO}_4$ ($0.0 \leq x \leq 1.0$) ceramics. It is seen that the two bands at 316 cm^{-1} and 357 cm^{-1} , which are assigned to $\delta_{\text{as}}(\text{VO}_4)$ mode and the $\delta_{\text{s}}(\text{VO}_4)$, respectively, moved closer to each other with the increase of x value and finally merged into one band at around $x = 0.10$. Furthermore, the bands below 200 cm^{-1} (at least three) for pure BiVO_4 broadened and gradually overlapped with the increase of x value, and then could not be distinguished from each other at $x = 0.10$. All these phenomena reflect the increase of the degree of symmetry.

To further study the intrinsic microwave dielectric properties, the IR reflectivity spectra of $x\text{Bi}_{2/3}\text{MoO}_4-(1-x)\text{BiVO}_4$ ($0.0 \leq x \leq 1.0$) ceramics were analyzed using a classical harmonic oscillator model as follows:

$$\varepsilon^*(\omega) = \varepsilon_\infty + \sum_{j=1}^n \frac{\omega_{pj}^2}{\omega_{oj}^2 - \omega^2 - j\gamma_j\omega} \quad (1)$$

where $\varepsilon^*(\omega)$ is complex dielectric function; ε_∞ is the dielectric constant caused by the electronic polarization at high frequencies; γ_j , ω_{oj} , and ω_{pj} are the damping factor, the transverse frequency, and plasma frequency of the j -th Lorentz oscillator, respectively;

and n is the number of transverse phonon modes. The complex reflectivity $R(\omega)$ can be written as:

$$R(\omega) = \left| \frac{1 - \sqrt{\varepsilon^*(\omega)}}{1 + \sqrt{\varepsilon^*(\omega)}} \right|^2 \quad (2)$$

The fitted IR reflectivity values were shown in Fig. 6, and the complex permittivities are shown in Fig. 7. It is seen that all the calculated dielectric permittivity and dielectric loss values are almost equal to the measured ones using $TE_{01\delta}$ method, which implies that majority of the dielectric contribution for this system at microwave region was attributed to the absorptions of structural phonon oscillation at infrared region and very little contribution from defect phonon scattering. The Phonon parameters obtained from the fitting of the infrared reflectivity spectra of $x\text{Bi}_{2/3}\text{MoO}_4-(1-x)\text{BiVO}_4$ ($x=0.00$, $x=0.06$, $x=0.08$, and $x=0.10$) ceramics are listed in Table I and II. It can be seen that the dielectric polarization contribution from the vibration modes below 150 cm^{-1} can reach above 75 % of the total value for $x=0.00$, 0.06, 0.08, and 0.10 sample, and it is quite different from the result of pure $\text{Bi}_{2/3}\text{MoO}_4$ (about 5 % from the first mode, and the detailed data are not shown here). This implies that the dielectric polarization contribution of monoclinic scheelite solid solution comes from the external modes, which means the vibrational modes of Bi-O stretches. However, due to the overlapping of modes at low wave number, the accuracy of calculated permittivity was influenced by the errors from the fitting. It is understandable that the neighboring structure of Bi^{3+} can account for the change of macroscopical permittivity due to its large polarization about 6.12 \AA^3 , which is much larger than that of Mo^{6+} and V^{5+} ions (3.28 \AA^3 and 2.92 \AA^3 , respectively). Hence, although the overlapping of $\delta_{\text{as}}(\text{VO}_4)$ mode and the $\delta_s(\text{VO}_4)$, corresponding to the ferroelastic phase transition, can be obviously observed both from Raman and IR

spectra, their dielectric polarization contribution to the microwave permittivity were quite low, and the influence could be ignored.

IV. Conclusions

The full composition of $x\text{Bi}_{2/3}\text{MoO}_4-(1-x)\text{BiVO}_4$ ($0.0 \leq x \leq 1.0$) ceramics were prepared via the solid state reaction method. The phase diagram of the whole system can be separated into at least four regions in the temperature below the melting points: I, scheelite monoclinic phase region with $0.0 \leq x \leq 1.0$; II, scheelite tetragonal phase region with $0.1 < x < 0.5$; III, an ordered scheelite phase region with $0.5 \leq x < 0.7$; IV, composite phase region with $0.7 \leq x < 1.0$ (ordered scheelite and monoclinic $\text{Bi}_{2/3}\text{MoO}_4$ phase). The characteristic overlapping of $\delta_s(\text{VO}_4)$ (B_g) and $\delta_{as}(\text{VO}_4)$ (A_g) modes during the ferroelastic phase transition could be observed in Raman spectra. Excellent microwave dielectric properties with permittivity around 75 and Qf value around 8,000 GHz could be obtained in the compositions near the phase boundary ($x = 0.10$) of monoclinic and tetragonal scheelite phases. It can be concluded that the polarization contribution at microwave region is dominated by the Bi-O stretches in $x\text{Bi}_{2/3}\text{MoO}_4-(1-x)\text{BiVO}_4$ ($0.0 \leq x \leq 1.0$) when $x \leq 0.10$ from the intrinsic results calculated from the fitting data of far infrared spectra. Hence, it would be an effective way to improve the microwave dielectric properties of bismuth based scheelite ceramics by modifying the A-site occupation and ions.

Acknowledgements

This work was supported by National Science Foundation of China (51202182, 51202178), the Fundamental Research Funds for the Central University, the international cooperation project of Shaanxi Province (2013KW12-04), the State Key

Laboratory of New Ceramic and Fine Processing Tsinghua University and the 111 Project of China (B14040). The author would like to thank Qiu-Ping Wang, Han-Chen Liu, and Chao Zhou for their help in Raman experimental and the administrators in IR beamline workstation of National Synchrotron Radiation Laboratory (NSRL) for their help in the IR measurement. The SEM work was partially done at International Center for Dielectric Research (ICDR), Xi'an Jiaotong University, Xi'an, China and the authors thank Ms. Lu Lu and Ms. Yan-Zhu Dai for their help in using TEM and SEM. We also wish to thank the National Science Foundation I/UCRC program, as part of the Center for Dielectric Studies under Grant No. 0628817, for partial support and also the MCL facilities at Penn State University.

Reference

- 1 M. T. Sebastian, H. Jantunen, *Int. Mater. Rev.*, 2008, **53**, 57.
- 2 R. J. Cava, *J. Mater. Chem.*, 2001, **11**, 54.
- 3 D. Zhou, H. Wang, L. X. Pang, C. A. Randall, X. Yao, *J. Am. Ceram. Soc.*, 2009, **92**, 2242.
- 4 D. K. Kwon, M. T. Lanagan, T. R. Shrout, *J. Am. Ceram. Soc.*, 2005, **88**, 3419.
- 5 . Udovic, M. Valant, D. Suvorov, *J. Am. Ceram. Soc.*, 2004, **87**, 591.
- 6D. Zhou, L. X. Pang, J. Guo, Z. M. Qi, T. Shao, X. Yao, C. A. Randall, *J. Mater. Chem.*, 2012, **22**, 21412.
- 7 M. Valant, D. Suvorov, *J. Am. Ceram. Soc.*, 2000, **83**, 2721.
- 8 R. D. Shannon, *J. Appl. Phys.*, 1993, **73**, 348.
- 9 X. L. Wang, H. Wang, X. Yao, *J. Am. Ceram. Soc.*, 1997, **80**, 2745.
- 10 D. Zhou, H. Wang, X. Yao, L. X. Pang, *Ceram. Int.*, 2008, **34**, 901.
- 11 L. Tong, A. Iwase, A. Nattestad, U. Bach, M. Weideler, G. Götz, A. Mishra, P. Bäuerle, R. Amal, G. G. Wallace, A. J. Mozer, *Energy Environ. Sci.*, 2012, **5**, 9472.
- 12 J. D. Bierlein, A. W. Sleight, *Solid State Commun.*, 1975, **16**, 69.
- 13 R. M. Hazen, J. W. E. Mariathasan, *Science*, 1982, **216**, 991.
- 14 D. Zhou, W. G. Qu, C. A. Randall, L. X. Pang, H. Wang, X. G. Wu, J. Guo, G. Q. Zhang, L. Shui, Q. P. Wang, H. C. Liu, X. Yao, *Acta Mater.*, 2011, **59**, 1502.
- 15 D. Zhou, L. X. Pang, H. Wang, J. Guo, X. Yao, C. A. Randall, *J. Mater. Chem.*, 2011, **21**, 18412.
- 16 D. Zhou, C. A. Randall, H. Wang, L. X. Pang, X. Yao, *J. Am. Ceram. Soc.*, 2010, **93**, 2147.
- 17 A. W. Sleight, W. J. Linn, *Ann. NY Acad. Sci.*, 1976, **272**, 22.

- 18 L. H. Brixner, A. W. Sleight, M. S. Liciš, *J. Solid State Chem.*, 1972, **5**, 247.
- 19 W. Jeitschko, *Acta Crystallogr.*, 1973, **B29**, 2074.
- 20 A. W. Sleight, K. Aykan, D. B. Rogers, *J. Solid State Chem.*, 1975, **13**, 231.
- 21 F. Theobald, A. Laarif, A. W. Sleight, *Mater. Res. Bull.*, 1985, **20**, 653.
- 22 F. D. Hardcastle, I. E. Wachs, *J. Phys. Chem.*, 1991, **26**, 10763.
- 23 A. V. Ghule, K. A. Ghule, S. H. Tzing, J. Y. Chang, H. Chang, Y. C. Ling, *Chem. Phys. Lett.*, 2004, **383**, 208.
- 24 T. Ono, N. Ogata, R. L. Kuczkowski, *J. Catal.*, 1998, **175**, 185.
- 25 G. K. Choi, J. R. Kim, S. H. Yoon, K. S. Hong, *J. Eur. Ceram. Soc.*, 2007, **27**, 3063.

Table I. Phonon parameters obtained from the fitting of the infrared reflectivity spectra of $x\text{Bi}_{2/3}\text{MoO}_4-(1-x)\text{BiVO}_4$ ($x=0.00$ and 0.060) ceramics

Mode	ω_{oj}	ω_{pj}	γ_j	$\Delta\epsilon_j$	Mode	ω_{oj}	ω_{pj}	γ_j	$\Delta\epsilon_j$
1	75.09	509.75	18.80	46.1	1	72.32	536.12	22.58	55
2	101.18	334.49	17.97	10.9	2	98.16	289.03	24.39	8.67
3	127.16	111.26	12.06	0.77	3	135.49	75.47	14.60	0.31
4	144.34	84.72	8.88	0.35					
5	213.18	182.22	57.50	0.73	4	211.63	232.38	50.06	0.39
6	280.06	183.40	34.41	0.43	5	272.86	184.21	40.46	0.46
7	315.59	124.98	23.30	0.16	6	317.58	134.63	24.46	0.18
8	356.92	240.33	33.32	0.45	7	346.42	224.71	47.32	0.42
9	407.15	173.49	29.96	0.18	8	406.43	229.45	45.14	0.32
10	472.24	371.50	85.37	0.62	9	482.32	350.23	94.85	0.52
11	560.48	477.86	86.15	0.73	10	565.87	450.3	91.65	0.63
12	625.27	693.64	82.15	1.23	11	630.24	672.97	95.66	1.14
13	696.63	403.49	89.51	0.34	12	711.71	411.74	12244	0.34
14	799.23	149.46	46.86	0.04					
$x=0.00$	$\epsilon_\infty=3.95$		$\epsilon_0=63.03$		$x=0.06$	$\epsilon_\infty=3.59$		$\epsilon_0=68.38$	

Table II. Phonon parameters obtained from the fitting of the infrared reflectivity spectra of $x\text{Bi}_{2/3}\text{MoO}_4-(1-x)\text{BiVO}_4$ ($x = 0.08$ and 0.10) ceramics

Mode	ω_{oj}	ω_{pj}	γ_j	$\Delta\epsilon_j$	Mode	ω_{oj}	ω_{pj}	γ_j	$\Delta\epsilon_j$
1	70.57	524.74	21.56	55.3	1	81.08	610.30	23.34	56.70
2	94.31	275.34	23.39	8.52	2	106.02	272.35	31.18	6.60
3	127.34	69.07	15.13	0.29					
4	210.69	126.04	49.34	0.36	3	209.86	135.68	50.04	0.42
5	269.37	172.38	37.23	0.41	4	270.22	170.28	32.68	0.40
6	329.01	278.83	57.22	0.72	5	329.60	267.83	46.71	0.66
7	404.65	272.83	57.89	0.46	6	407.65	293.72	59.98	0.52
8	487.02	369.92	92.81	0.58					
9	562.43	446.24	88.24	0.63	7	531.67	488.90	120.98	0.85
10	624.43	572.97	95.54	0.84	8	627.85	845.65	101.39	1.81
11	710.39	338.38	119.96	0.23	9	714.65	475.56	109.01	0.44
x=0.08	$\epsilon_\infty=3.05$		$\epsilon_0=68.34$		x=0.10	$\epsilon_\infty=4.41$		$\epsilon_0=68.40$	

Figure Captions:

Fig. 1. X-ray diffraction patterns for $x\text{Bi}_{2/3}\text{MoO}_4-(1-x)\text{BiVO}_4$ ($0.0 \leq x \leq 1.0$) ceramics sintered at different temperatures (a) (the merging of (1 0 1) and (0 1 1), (2 0 0) and (0 2 0) was marked by dash line), (b) (the super-lattice diffraction peaks were marked), (c), the cell parameters of scheelite phase as a function of x value (d) (the four regions were distinguished by the cell parameters), the schematic structure (e) of BiVO_4 (top) and $\text{Bi}_{2/3}\text{MoO}_4$ (bottom) with only half the unit cell shown in *ab*-plane (\circ -tetragonal scheelite phase, $*$ - $\text{Bi}_{2/3}\text{MoO}_4$ monoclinic phase) and a set of selected area electron diffraction patterns recorded from the BVM0.35 sample (f).

Fig. 2. SEM photos of as-fired surfaces of BVM0.06 ceramic sintered at 830 °C/2hrs (a), BVM0.08 ceramic sintered at 830 °C/2hrs (b), BVM0.10 ceramic sintered at 780 °C/2hrs (c), and fractured surfaces of BVM0.35 ceramic sintered at 680 °C/2hrs (d), BVM0.65 ceramic sintered at 650 °C/2hrs (e), and BVM1.00 ceramic sintered at 620 °C/2hrs (f)

Fig. 3. Room temperature Raman spectra of $x\text{Bi}_{2/3}\text{MoO}_4-(1-x)\text{BiVO}_4$ ($0.0 \leq x \leq 1.0$) ceramics (a) and *in situ* Raman spectra of BVM0.06 sample in the temperature range 25 °C ~ 200 °C

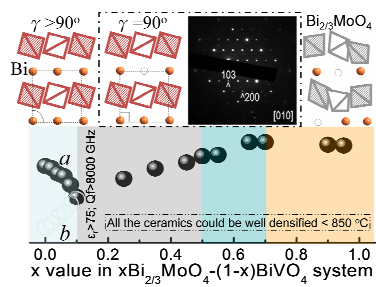
Fig. 4. Room temperature microwave dielectric permittivity and Qf values of $x\text{Bi}_{2/3}\text{MoO}_4-(1-x)\text{BiVO}_4$ ($0.0 \leq x \leq 1.0$) ceramics as a function of x value

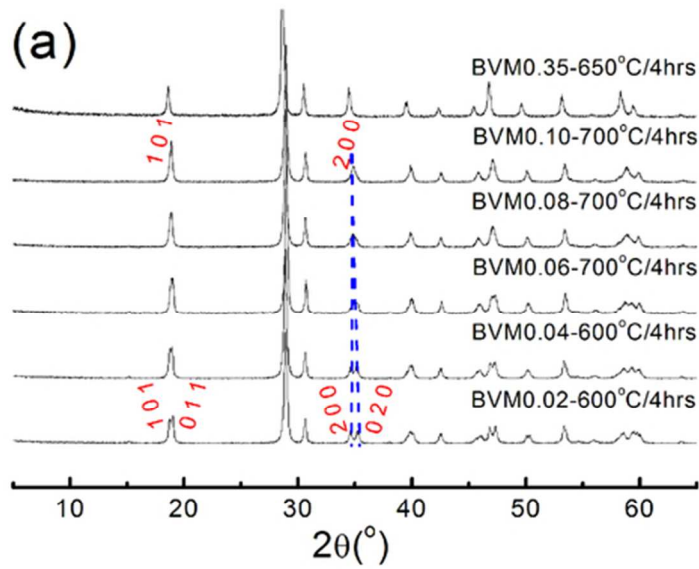
Fig. 5. Microwave dielectric permittivity (a) and Qf value (b) of $x\text{Bi}_{2/3}\text{MoO}_4-(1-x)\text{BiVO}_4$ ($x = 0.06, x = 0.08, x = 0.10$ and $x = 0.35$) ceramics as a function of temperature (-260 °C ~ +150 °C)

Fig. 6. Measured and calculated infrared reflectivity spectra of the $x\text{Bi}_{2/3}\text{MoO}_4-(1-x)\text{BiVO}_4$ ($0.0 \leq x \leq 1.0$) ceramics (solid line for fitting values and circle for measured values)

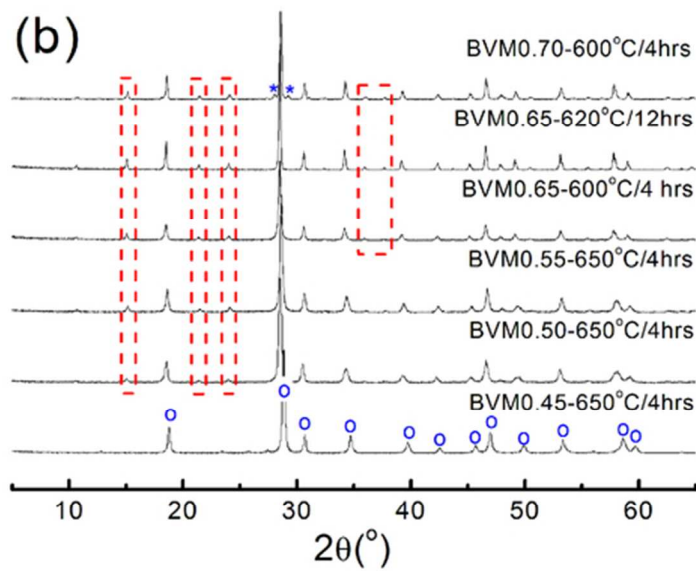
Fig. 7. Calculated and measured complex permittivity of the $x\text{Bi}_{2/3}\text{MoO}_4-(1-x)\text{BiVO}_4$ ($0.0 \leq x \leq 1.0$) ceramics for $x = 0.00, 0.06, 0.08, 0.10$ (a) and $x = 0.35, 0.65, 0.90, 1.00$ (b)

High permittivity and Qf value could be obtained near phase boundaries of monoclinic and tetragonal scheelite phases in $x\text{Bi}_{2/3}\text{MoO}_4-(1-x)\text{BiVO}_4$ ceramics.

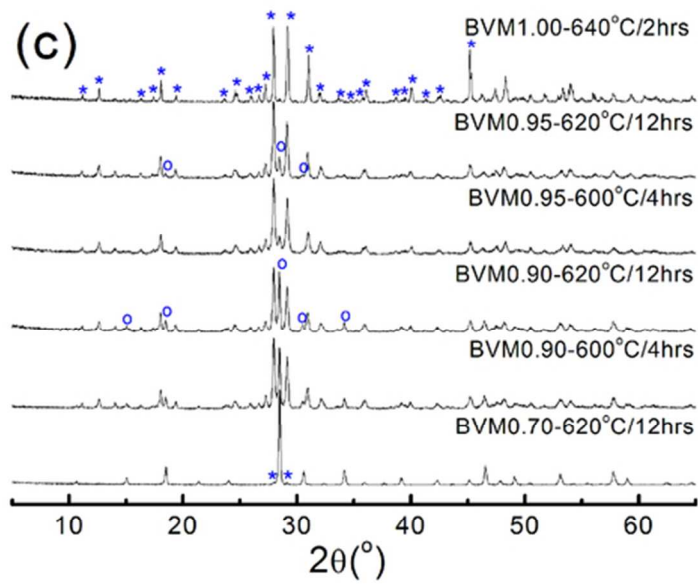




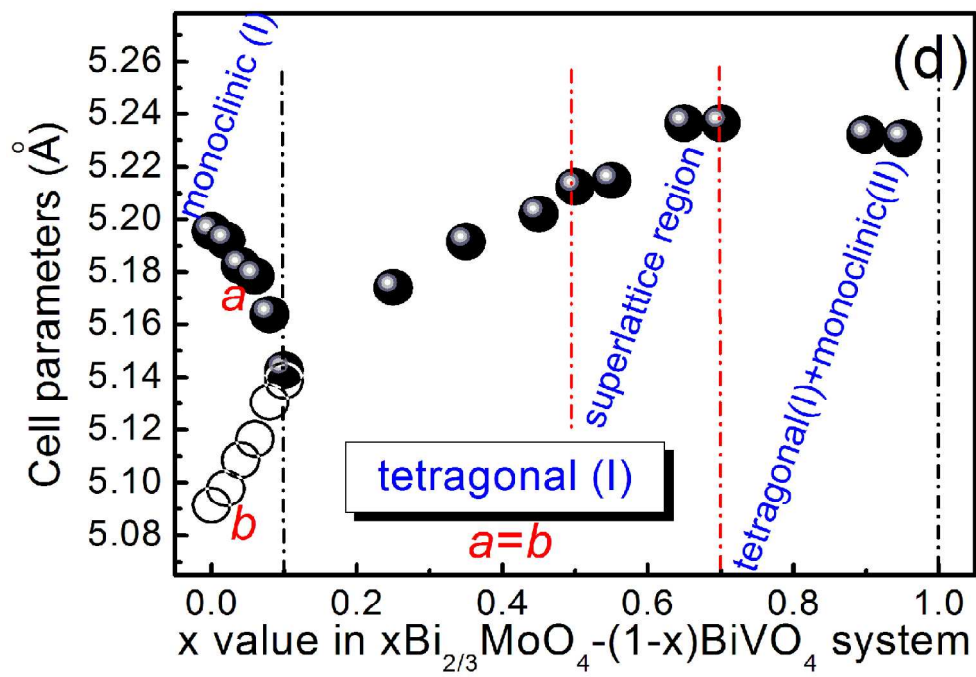
56x37mm (300 x 300 DPI)



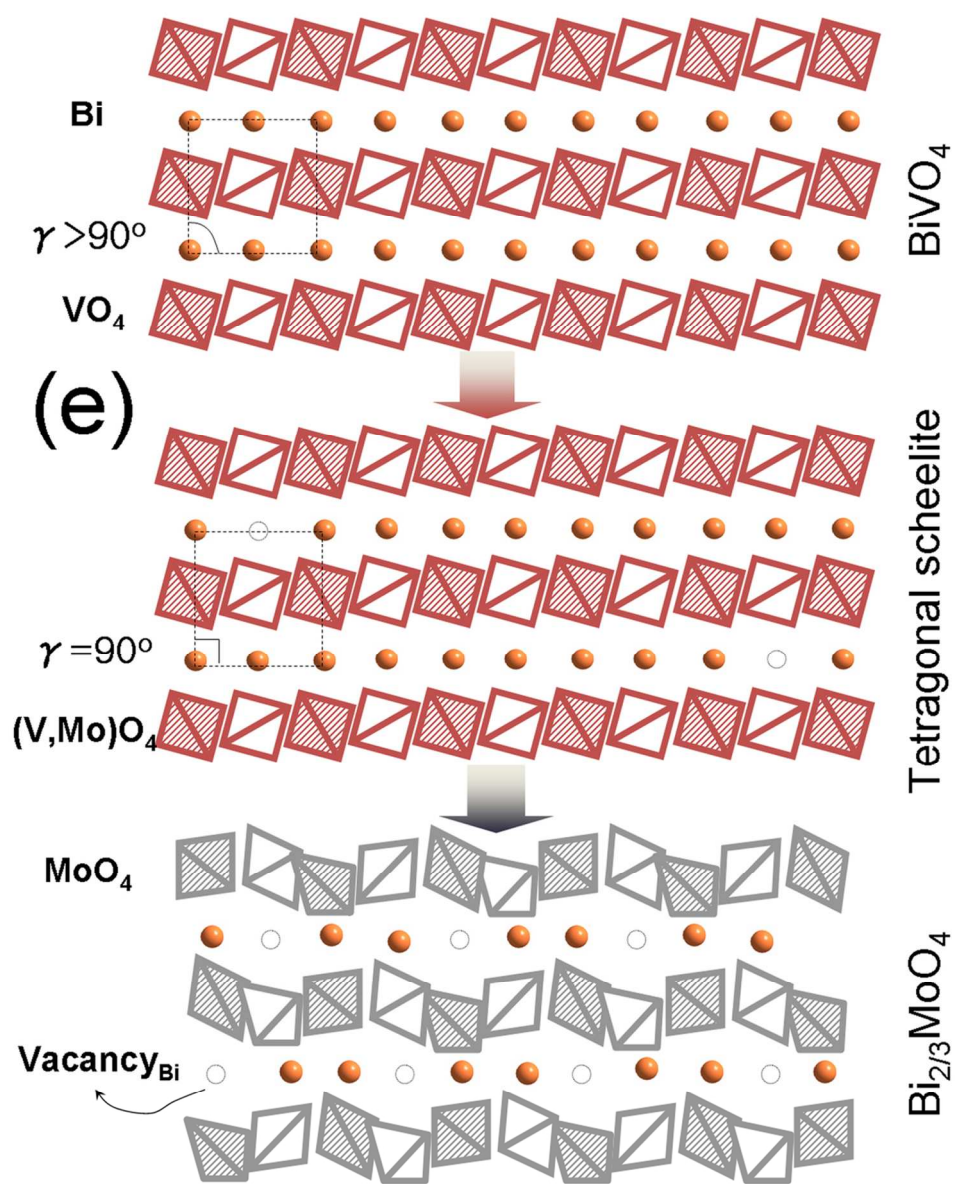
56x37mm (300 x 300 DPI)



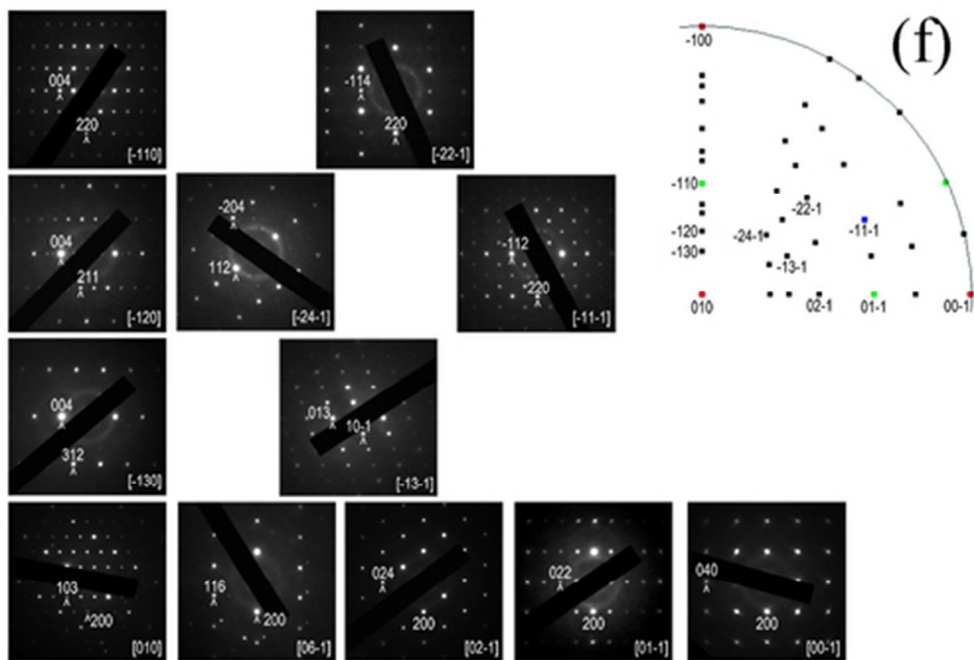
56x37mm (300 x 300 DPI)



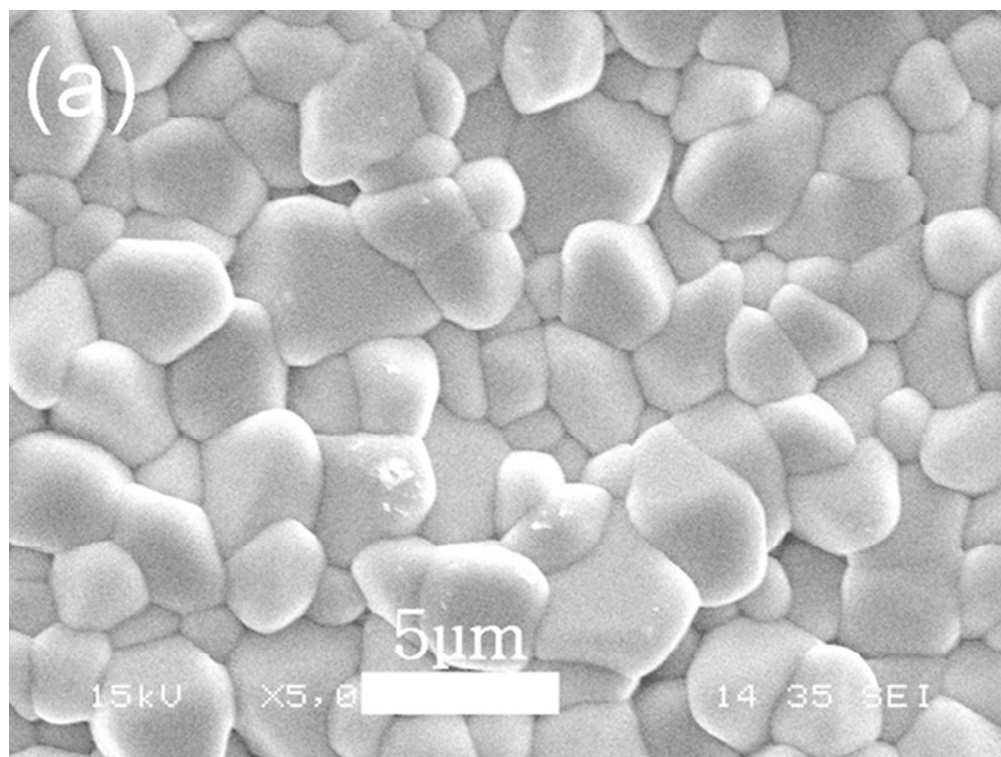
254x180mm (300 x 300 DPI)



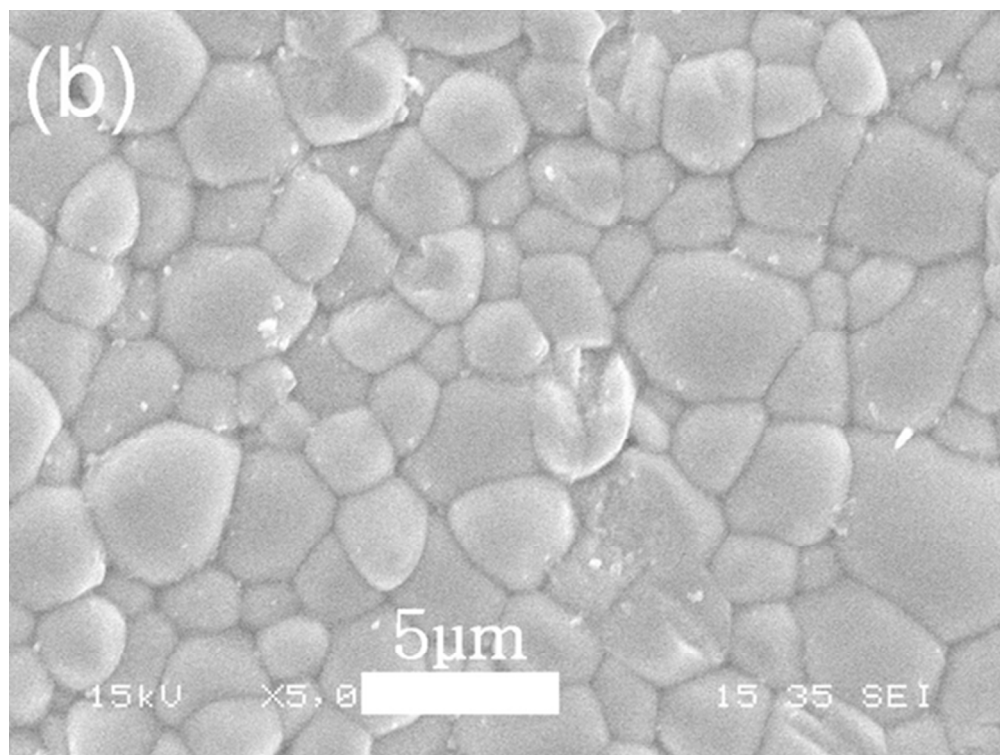
104x130mm (300 x 300 DPI)



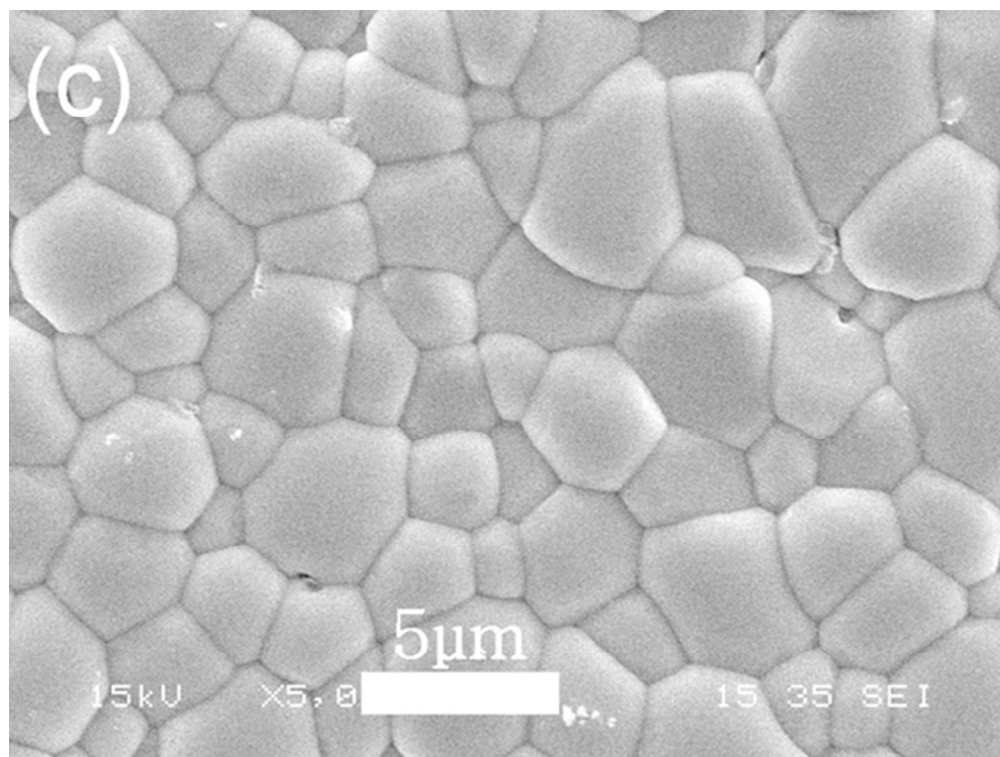
42x29mm (300 x 300 DPI)



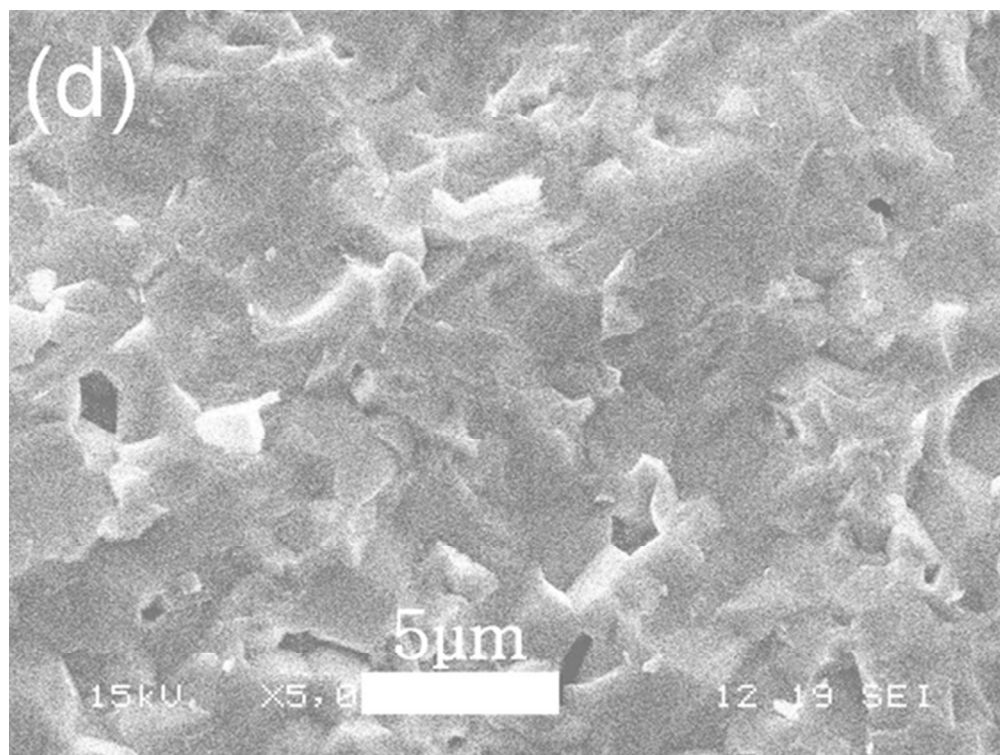
47x35mm (300 x 300 DPI)



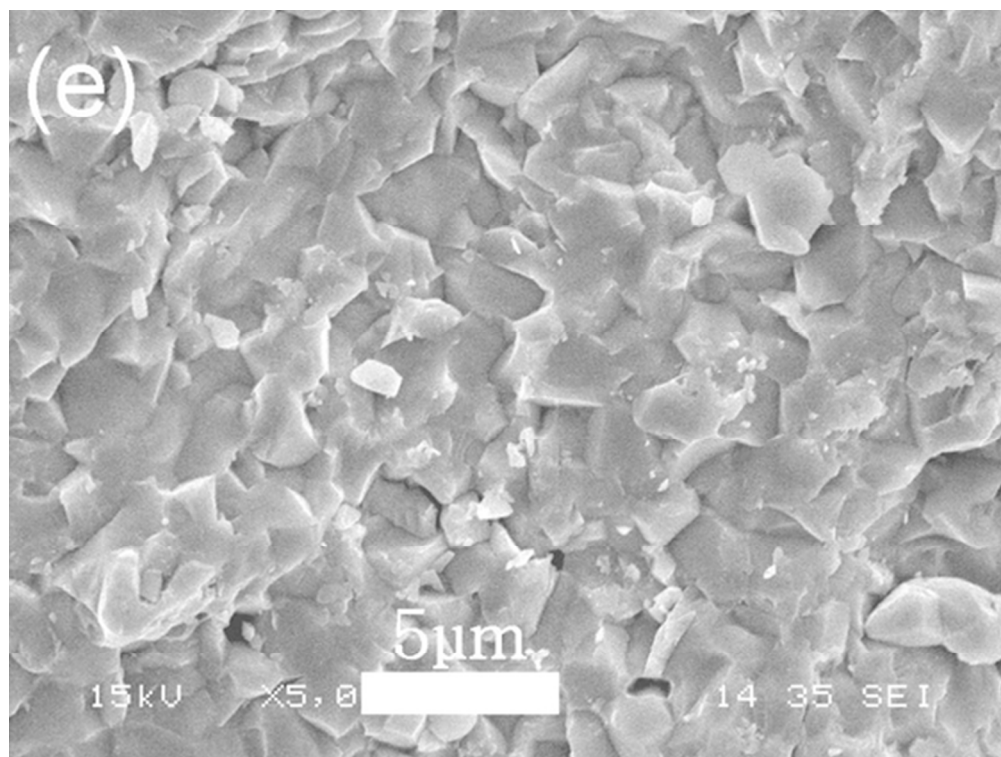
47x35mm (300 x 300 DPI)



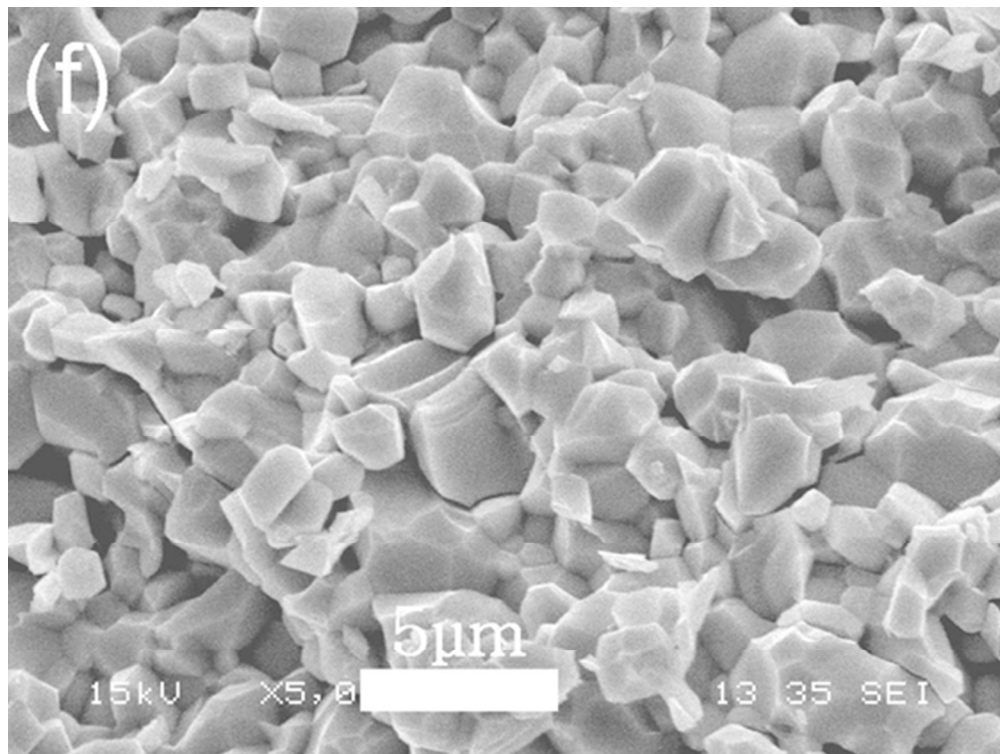
47x35mm (300 x 300 DPI)



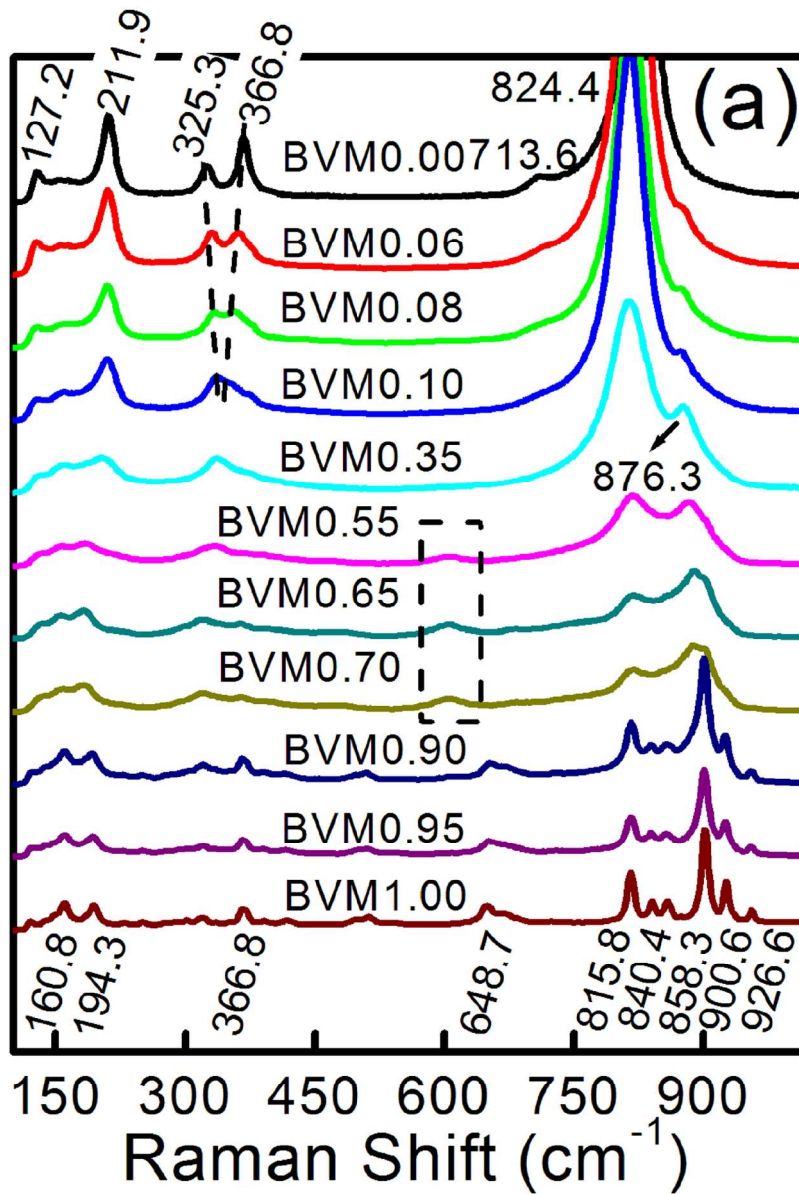
47x35mm (300 x 300 DPI)



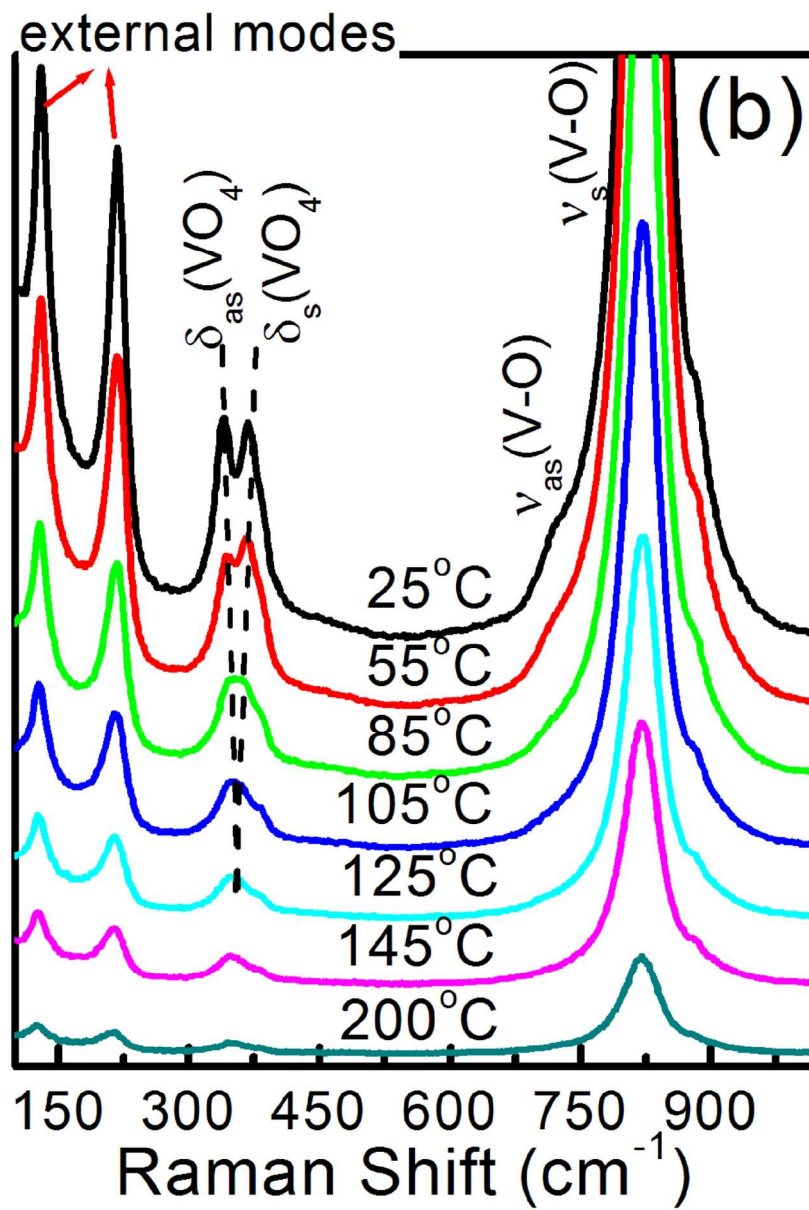
47x35mm (300 x 300 DPI)



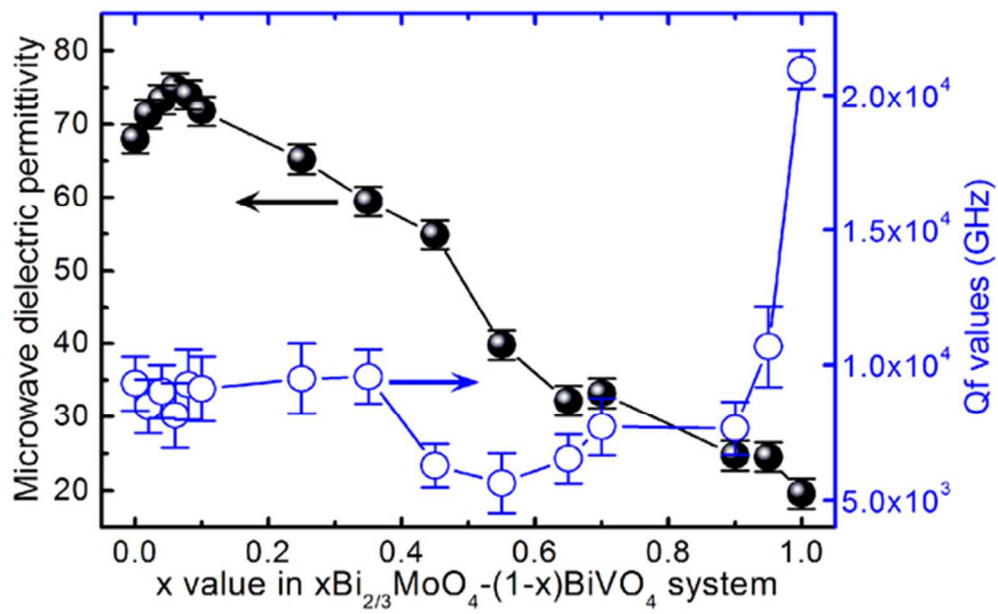
47x35mm (300 x 300 DPI)



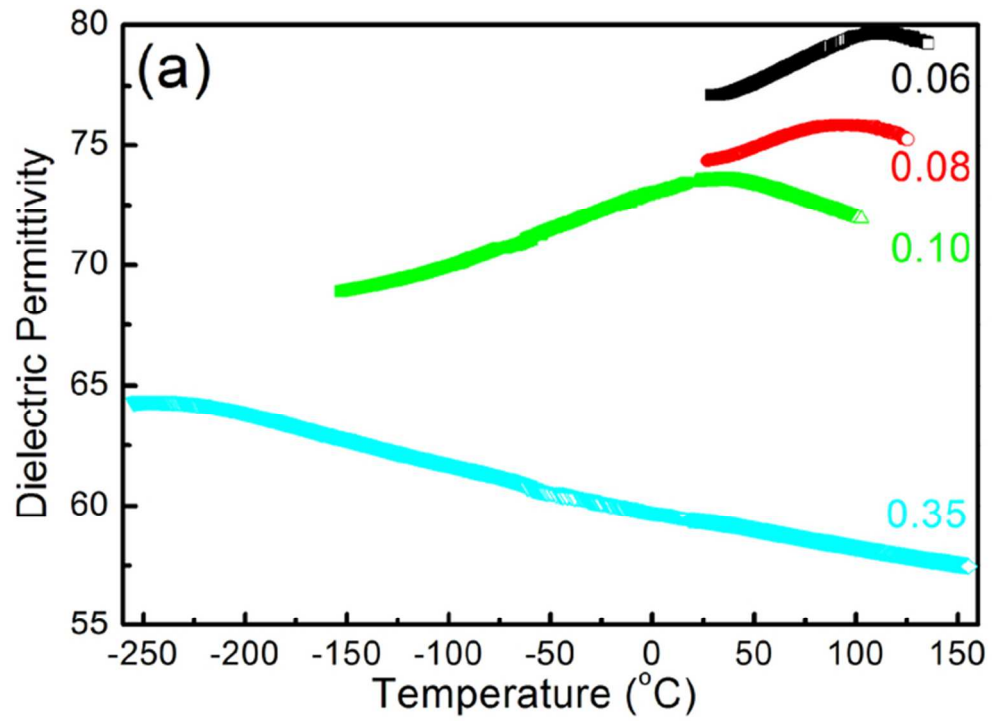
120x172mm (300 x 300 DPI)



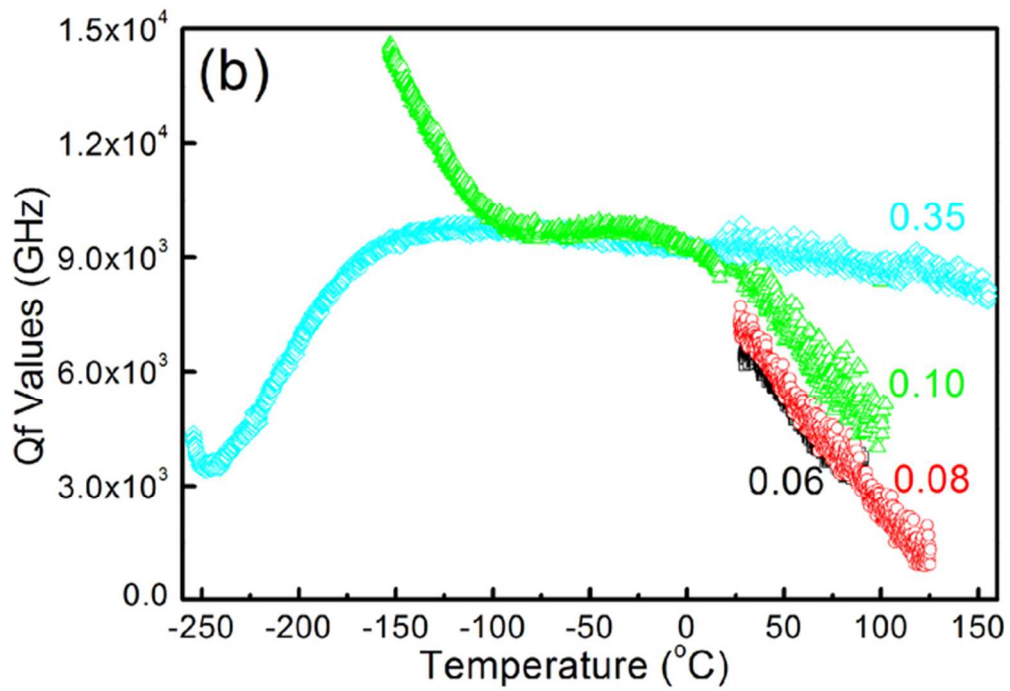
120x172mm (300 x 300 DPI)



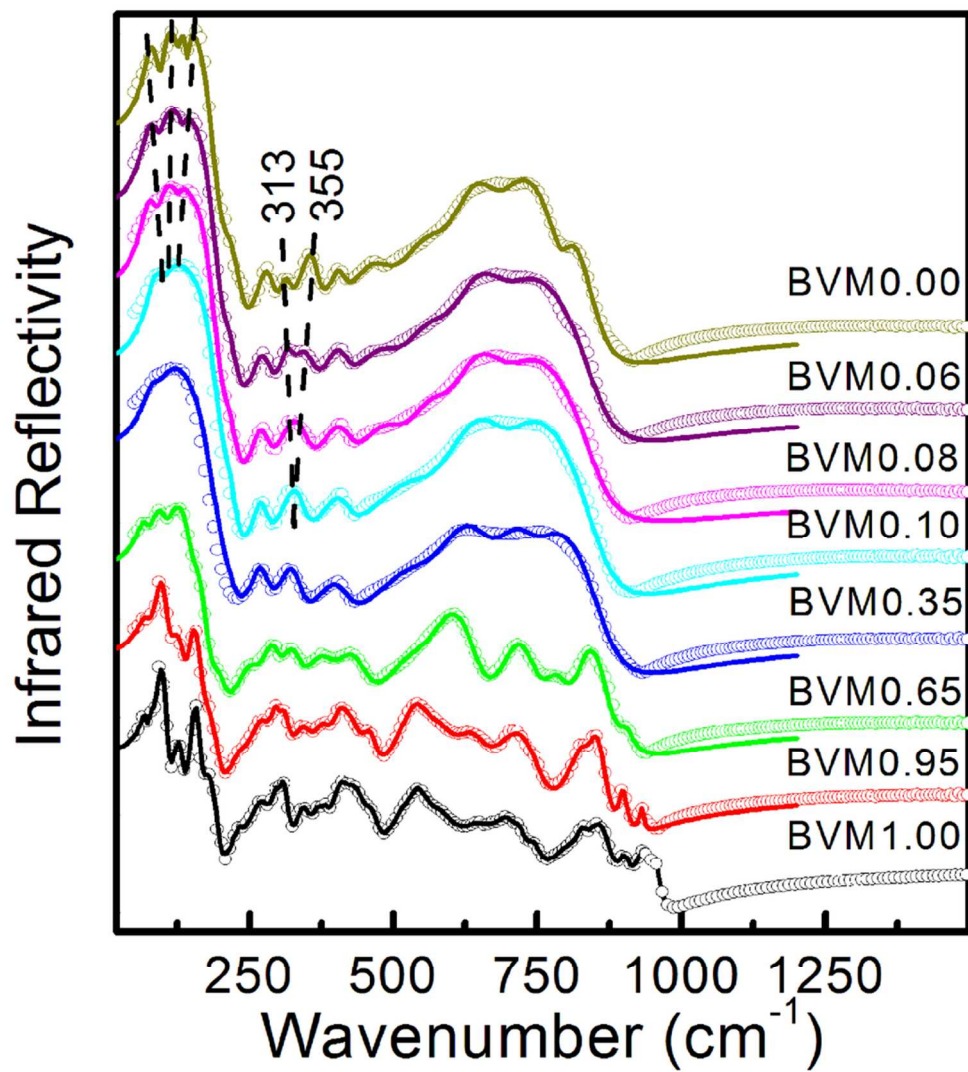
52x33mm (300 x 300 DPI)



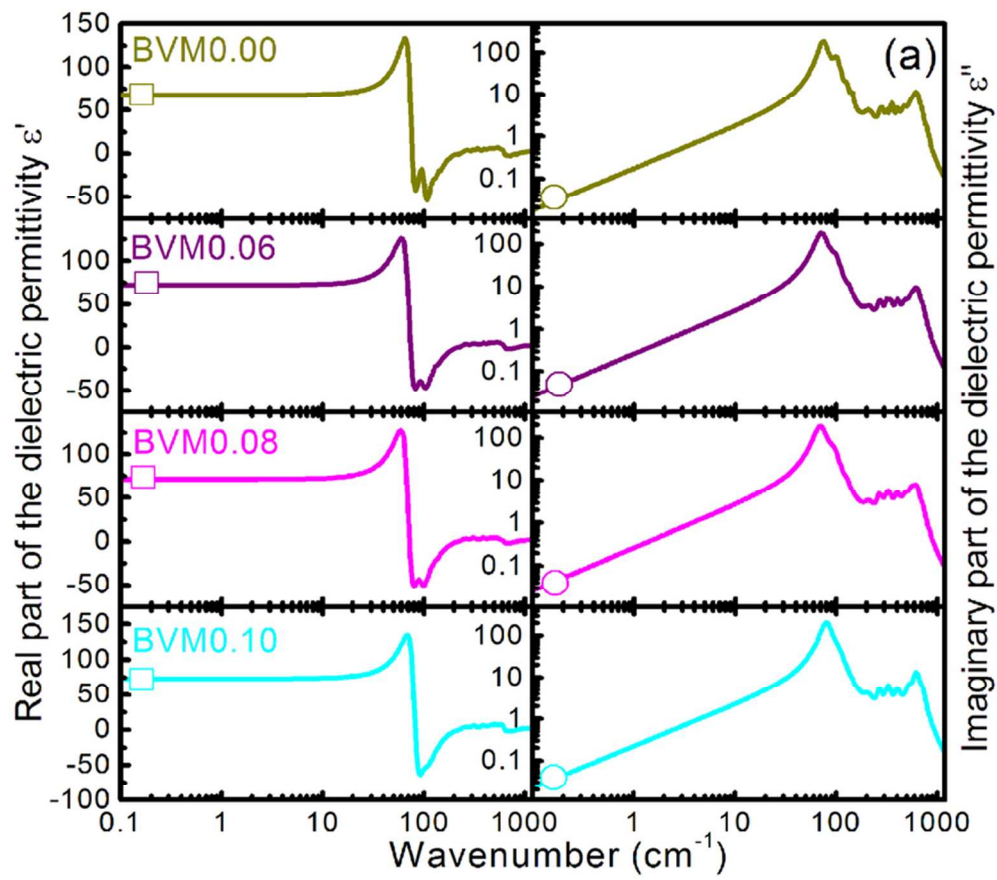
60x43mm (300 x 300 DPI)



57x39mm (300 x 300 DPI)



90x97mm (300 x 300 DPI)



74x65mm (300 x 300 DPI)

